Materials Advances

ROYAL SOCIETY OF CHEMISTRY

PAPER

View Article Online
View Journal | View Issue

Cite this: *Mater. Adv.*, 2022, 3, 5476

Zinc-coordinated polydopamine surface with a nanostructure and superhydrophilicity for antibiofouling and antibacterial applications†

Po Wang,[a] Yi-Lin Zhang,[a] Kai-Lai Fu,[a] Zhuang Liu, *[ab] Ling Zhang,[c] Chen Liu,[c] Yi Deng,[ab] Rui Xie,[ab] Xiao-Jie Ju,[ab] Wei Wang[ab] and Liang-Yin Chu[ab]

Received 29th April 2022,
Accepted 24th May 2022

DOI: 10.1039/d2ma00482h

rsc.li/materials-advances

Effective approaches are urgently needed to avoid the formation of thrombosis and bacterial infections during long-time intravenous implanation. Of particular importance are the surfaces of implants that not only satisfy the demand of an antibiofouling ability to repel thrombocytes, proteins, and bacteria, but also provide an antibacterial property without cytotoxicity to normal cells, which would be biosafe to blood. Here, we explore the implementation of such antibiofouling and antibacterial functions in a superhydrophilic nanostructured surface containing zinc-coordinated polydopamine (PDA/Zn). The formation mechanism of the zinc-coordinated polydopamine nanostructure was demonstrated with the growth and intertwining of the PDA/Zn nanowires *via* Zn–N and Zn–O bonds. The PDA/Zn nanostructured surface inhibited the attachment of biological substances, such as blood platelets and bovine serum albumin, as well as possessing excellent antibacterial properties. This work reports the fabrication mechanism of a PDA/Zn surface with a nanostructure and superhydrophilicity, which has potential for preventing biomaterial-associated biofouling and infections.

Introduction

Long-time intravenous implants and devices are a common and indispensable part of medical care and have had a great impact on patient health for both diagnostic and therapeutic purposes.[1–3] However, lots of risks come along with the implantable devices in veins, which could end up in a complete malfunctioning of the implant.[2,4,5] In general, thrombocytes that adhere on the surface of the implants can be activated to form local thrombosis.[6–9] To the implanted materials, thrombocytes adhering to their surfaces are actually considered biofouling,[7] just like bacterial infections. If planktonic bacterium attaches on the biomaterial surface, it may start to colonize.[10,11] Subsequently, a biofilm would be formed with complex and dynamic structures and would irreversibly attach by producing an extracellular matrix.[2,10,11] In case of no or delayed treatment, this process can end up in an acute infection, potentially causing implant failure and requiring replacement surgery, incurring a significant economic burden.[12] Compared to planktonic bacteria, biofilms possess lower susceptibility towards antimicrobials and host defence mechanisms, and therefore are challenging to treat.[13–15] Thus, preventing the biofouling of initial thrombocytes and bacterial attachment is crucial to avoiding the formation of further thrombosis and a biofilm, which could influence implant-associated infections and implant failures.

A promising strategy to combat the biofouling adhesion of thrombocytes and bacteria is based on the functional surface of the implants, characterized by antibiofouling coatings[16,17] or antibacterial coatings.[5,18,19] Usually, the former type attracts much interest with the aim to inhibit the initial biofouling attachment on the surface through promoting low adhesion or even repellent properties towards thrombocytes, proteins, and bacteria.[16] Recently, a superhydrophilic nanostructure surface that exhibited a water contact angle lower than 10° was proposed for achieving the antibiofouling goal through means other than imparting lubricity to the implants.[20,21] Because the affinity between the surface and water molecules is strong, on such a surface, water spreads to form a continuous water film, which acts as a barrier to prevent interactions between the biofouling and the surface, thus resisting biofouling adhesion.[22,23]

[a] *School of Chemical Engineering, Sichuan University, Chengdu, Sichuan 610065, P. R. China. E-mail: liuz@scu.edu.cn*
[b] *State Key Laboratory of Polymer Materials Engineering, Sichuan University, Chengdu, Sichuan 610065, P. R. China*
[c] *Kidney Research Institute, Division of Nephrology, West China Hospital of Sichuan University, Chengdu, Sichuan 610065, China*

† Electronic supplementary information (ESI) available: The Water contact angle, SEM images and high-resolution XPS spectra of N1s of PU and PU-PDA films; the FT-IR spectrum of PU-PDA and PU-PDA/Zn films; the possible structures of Zn^{2+} bonding with polydopamine *via* Zn–N and Zn–O bonds; SEM images of the platelets adhered on PU (a), PU-PDA (b), PU-PDA/Zn-0.08 (PDF). See DOI: https://doi.org/10.1039/d2ma00482h

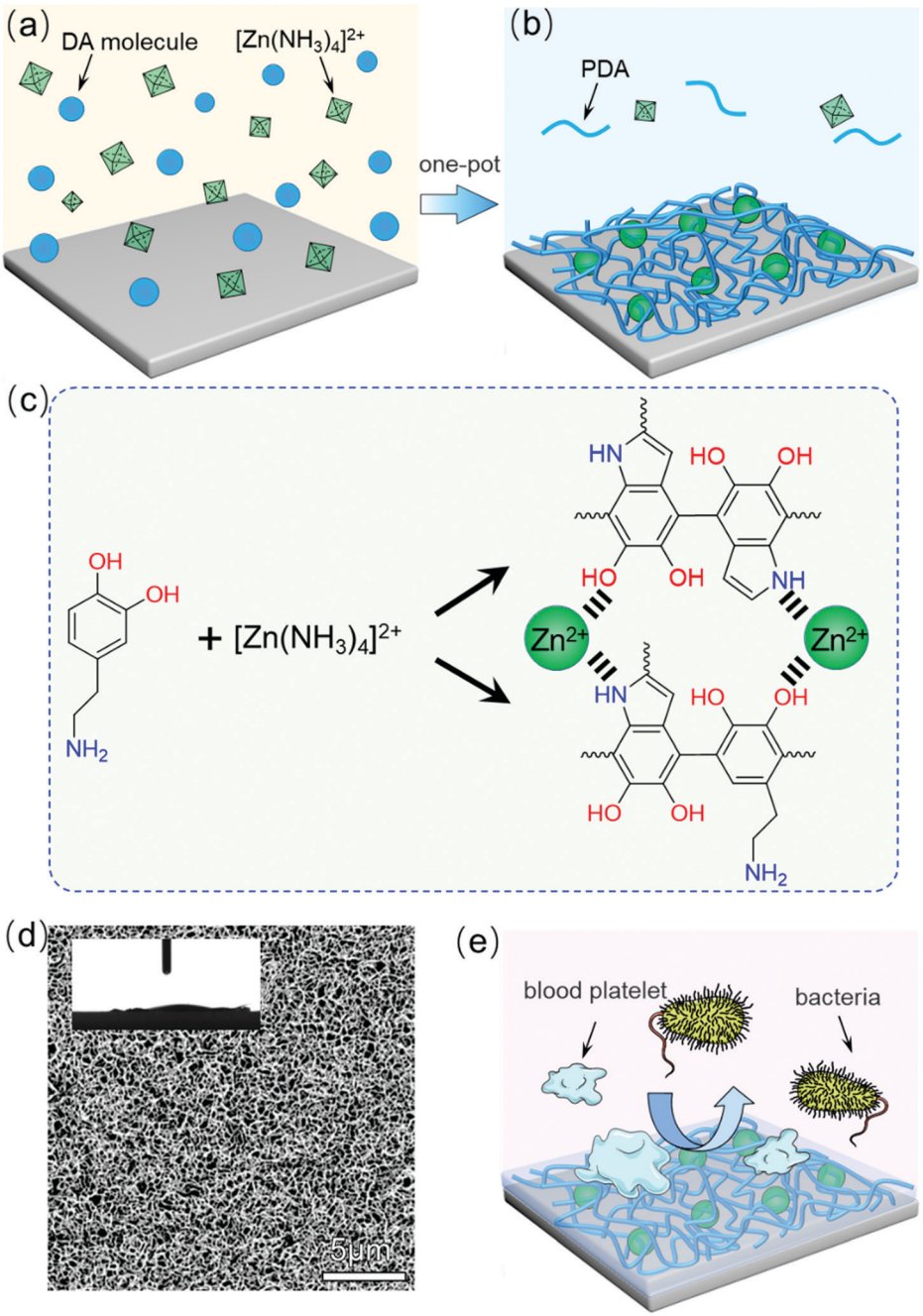

Fig. 1 Schematic illustration of the PU-PDA/Zn film preparation process. (a and b) Preparation of the PU-PDA/Zn coating by the dopamine one-pot method. (c) Schematic diagram of zinc ion and dopamine dimer complexation. (d) Nanostructure and superhydrophilicity of the PDA/Zn film surface. (e) Schematic diagram of the antibiofouling and antibacterial properties of the PDA/Zn film surface.

The surface modifications to engineer superhydrophilicity can be performed by changing the surface chemistry or topography using polymer-based hydrogels,[24,25] zwitterionic polymers,[26–28] or various hydrophilic polymer brushes,[29–31] which are able to provide an antibiofouling property but few of them possess an intrinsic bacterial-killing ability.[18] As another approach, antibacterial coatings are able to kill microbes when they approach the implants surfaces *via* contact-killing and release-killing models.[32,33] Such functional coatings can be created by confining antimicrobial substances at the biomaterial surfaces, where bacterial killing is supposed to occur due to the disruption of the cell membrane. For instance, quaternary-ammonium compounds are very well-known antimicrobial molecules and are commonly used to prepare contact-killing surfaces.[34–36] Alternatively, the direct localized release of an antimicrobial substance from the material surface offers the option for delivery only where needed, thus preventing the toxicity from reaching other parts of the body and minimizing resistance development. Silver, copper, and zinc are currently used

as releasable antibacterial agents.[37,38] However, silver antibacterial agents are not allowed in intravenous implants due to silver's biotoxicity.[39] Additionally, without repellent properties, biological elements, such as thrombocytes, protein, and DNAs, are still likely to adhere on the contact-killing or release-killing coatings if they do not have superhydrophilicity. Therefore, an ideal functional surface should not only satisfy the demand of an antibiofouling ability to repel the thrombocytes, protein, and bacteria, but should also provide an antibacterial property without cytotoxicity to normal cells and with biosafety to blood. However, the facile establishment of such multifunctional surfaces still remains a challenge.

Here, we report a zinc-coordinated polydopamine (PDA/Zn) surface with a nanostructure and superhydrophilicity, which combines both antibiofouling and antibacterial properties. The fabrication process is quite easy, as shown in Fig. 1(a) and (b). Selecting polyurethane (PU) as a substrate, the PDA/Zn surface was prepared on the substrate by shaking PU in a mixed solution with dopamine and zinc ammonium, since dopamine can self-polymerize with the release of hydrogen ions,[40] which subsequently react with zinc ammonium to promote weak neutralization. The zinc ions further coordinatively bonded with the –N and –O in the polydopamine (Fig. 1(c)). The zinc-coordinated polydopamine nanowires grew and became intertwined, resulting in the formation of the nanostructure of the surface, which was superhydrophilic (Fig. 1(d)). Thus, the PDA/Zn surface inhibited the attachment of biological substance, such as blood platelets and bovine serum albumin. On the other hand, zinc is known to have antibacterial properties, probably due to the irreversible Zn(II)–protein bindings.[41,42] Our nanostructured PDA/Zn surface possesses excellent antibacterial properties (Fig. 1(e)). This work provides a new platform for performing a simple and reliable surface design and optimization of the PDA/Zn coating processes to allow it to be potentially used in the biomedical field to prevent biomaterial-associated biofouling and infection.

Experimental section

Materials

Dopamine hydrochloride (DA·HCl) was purchased from Sigma-Aldrich (USA). Zinc chloride ($ZnCl_2$) and copper(II) sulfate pentahydrate ($CuSO_4{\cdot}5H_2O$, 99%), were obtained from Aladdin (China). The ammonium hydroxide was supplied by Chengdu KeLong Reagent Co., Ltd (China). The polyurethane (PU) film was obtained from Schweitzer–Mauduit (SWM) International, Inc. The bovine serum albumin (BSA) reagent was obtained from Beijing BaiAoLaiBo Technology Co., Ltd (China). The fetal bovine serum (FBS) was purchased from Gibco Life Technologies (USA). The live/dead BacLight Bacterial Viability Kit (L7012) was purchased from Invitrogen (USA), and the Cell Counting Kit-8 (CCK-8) was purchased from the Tongren Institute of Chemistry (China). The deionized water was obtained from a Milli-Q system (Millipore, USA). All the other chemical reagents were purchased from Aladdin (China) unless otherwise noted.

Preparation of PDA coating and PDA/Zn coating on the PU surface

Zinc ammonium complex was obtained by gradually adding 4 mol L^{-1} ammonia aqueous solution to 100 mL of 1 mol L^{-1} $ZnCl_2$ solution until the white floccules just disappeared. The concentration of the zinc ammonium complex was calculated as 0.435 mol L^{-1}. Zinc ammonium solutions with concentrations of 0.2, 0.15, 0.08, and 0.05 mol L^{-1} were obtained by diluting the 0.435 mol L^{-1} zinc ammonium solution. Next, 4 mL zinc ammonium solution with concentrations of 0.2, 0.15, 0.08, and 0.05 mol L^{-1} were poured into the vessel of a six-well cell plate, respectively. Followingly, 8 mg dopamine was added into one vessel to obtain 2 mg mL^{-1} dopamine mixed with zinc ammonium solution. Also, 2 mg mL^{-1} of dopamine solution without zinc ammonium (Tris–HCl, pH 8.4) was used as the control group. The PU film was cut into circular lamellas with a diameter of 1.75 cm, which were placed in the above-mentioned mixture solution. The reactions were carried out in a constant temperature shaking water bath at 25 °C with shaking in cycles of 85 rpm for different times (such as 1, 2, 6, and 24 h). The coated PU films were wished with DI water three times and then naturally dried.

Characterization

Scanning electron microscopy (SEM) images of the PU, PU-PDA, and PU-PDA/Zn films were obtained using a Phenom G2 Pro system (Phenom-World, Netherlands). The compositional analyses of the PU, PDA, and PU-PDA/Zn films were performed by Fourier-transform infrared spectroscopy (FT-IR) spectroscopy (Prestige-21, Shimadzu) using the total reflection method. X-ray photoelectron spectroscopy (XPS) was performed for the PU, PDA, and PU-PDA/Zn films using AlKα (1486.6 eV) as the radiation source (Kratos, XSAM800). The contact angles of the PU, PU-PDA, and PU-PDA/Zn films were analyzed using an interfacial tension meter (DSA25, Krüss GmbH Germany). For the PU-PDA/Zn membrane, atomic force microscopy (AFM) images were obtained on a MultiMode 8SPM microscope (BRUKER, German) to assess the mechanical properties.

Cytotoxicity and haemolysis tests

The cytotoxicity of the PU, PU-PDA, and PU-PDA/Zn films was verified by the viabilities of L929 mouse fibroblast cells. Here, 100 μL of the complete medium containing 2000 cells was added into one well of the 96-well plate. Next, 100 μg of the cut-up PU, PU-PDA, and PU-PDA/Zn films was added to each well to a final concentration of 0.1 mg mL^{-1}. The control group was set up without the films. The cells were cultured for 24 or 48 h at 37 °C and 5% CO_2. After the incubation, the medium was removed and replaced by another 90 μL of culture medium and 10 μL CCK-8 reagent for the following 4 h incubation. The absorbance was measured at 450 nm using a microplate reader (Multiskan FC, Thermo Fisher). The cell viability was calculated as the ratio of the absorbance of the tested samples to the control wells, as per the following:

$$\text{Cell viability} = (OD_{sample} - OD_{blank})/(OD_{control} - OD_{blank}) \times 100\%$$

where OD_{sample}, $OD_{control}$, and OD_{blank} are the optical densities (absorbance value) of the sample group, control group, and blank group. The blank group was the complete culture medium containing 1% double antibody and 10% calf serum (FBS). To ensure the accuracy of the experimental data, the optical density of the four wells was measured and averaged for each test group.

The PU, PU-PDA, and PU-PDA/Zn films with a diameter of 1.75 cm were placed in test tubes, respectively. Then, 10 mL normal saline was added in to each tube that was then put in to a water bath at 37 °C for 30 min. Next, 4 mL of rabbit whole blood containing sodium citrate was diluted with 5 mL of normal saline. Following, 0.2 mL of saline-diluted rabbit whole blood with sodium citrate was added into the sample-containing tubes, which were placed in a water bath at 37 °C for more than 1 h. After that, the solutions were centrifuged at a speed of 3000 rpm min^{-1} for 5 min. The absorbance value of the supernatants at the wavelength of 545 nm was determined using a microplate reader (Multiskan FC, Thermo Fisher). Three parallel samples for each group were tested to ensure the accuracy of the experimental data, while 10 mL normal saline was used for the negative control group, and 10 mL deionized water was used for the positive control group. The haemolysis ratio was calculated as follows:

$$\text{Haemolysis ratio} = (OD_t - OD_{nc})/(OD_{pc} - OD_{nc}) \times 100\%$$

where OD_t is the absorbance of the donor group (the experimental groups), OD_{nc} is the absorbance of the negative control group, and OD_{pc} is the absorbance of the positive control group.

Platelet and protein adsorption tests

The PU, PU-PDA, and PU-PDA/Zn films with a diameter of 1.75 cm were immersed overnight in isotonic phosphate buffer solution (PBS, pH 7.4). Platelet-rich plasma (PRP) from rabbit whole blood with sodium citrate was obtained by centrifugation at 1000 rpm for 10 min. The PU, PU-PDA, and PU-PDA/Zn films were subsequently immersed in 200 μL of concentrated PRP at 37 °C for 90 min. After that, the films were removed from the PRP, and washed by PBS solution three times. The washed films were treated with 2.5% glutaraldehyde for 4 h at room temperature. Then, the samples were dehydrated through 25, 50, 75, and 100 wt% ethanol–water solutions (10 min each time), and were dried for further use.

BSA as model proteins were selected to evaluate the protein adsorption analysis of the PU, PU-PDA, and PU-PDA/Zn films with a diameter of 1.75 cm, which were first immersed overnight in isotonic phosphate buffer solution (PBS, pH 7.4). The films were moved into BSA solution (1 mg mL^{-1}, 500 μL), respectively, and immersed at 37 °C for 2 h. Then, the BSA-adsorbed films were washed by PBS buffer solution and deionized water several times. All the film samples were sonicated in sodium dodecyl sulfate (SDS) (2 wt%, 500 μL) solution for 30 min to elute the surface-adsorbed proteins. (SDS solution can elute more than 95% adsorbed protein). Next, 25 μL of supernatant was added in to 200 μL of BCA working solution,

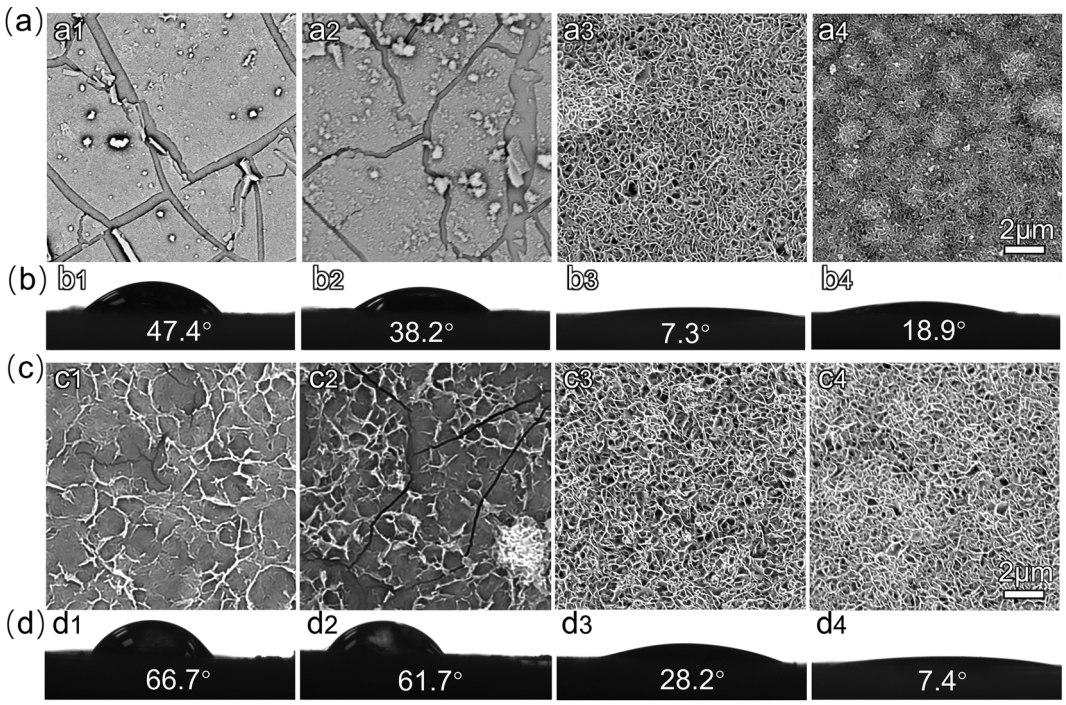

Fig. 2 SEM images (a) and water contact angle (b) of PU-PDA/Zn films prepared with 0.2 M (a1, b1), 0.15 M (a2, b2), 0.08 M (a3, b3), 0.05 M (a4, b4) zinc ammonium for 24 h. SEM images (c) and water contact angle (d) of PU-PDA/Zn-0.08 films after coating for 1 h (c1, d1), 2 h (c2, d2), 6 h (c3, d3), and 24 h (c4, d4).

and the absorbance at 545 nm of the mixed solution was measured by a microplate reader.

In vitro antibacterial properties

The UV-sterilized PU, PU-PDA, and PU-PDA/Zn films with a diameter of 1.75 cm were placed in a 24-well plate, and then 500 μL of bacteria (*Escherichia coli* or *Staphylococcus aureus*) diluted to 1.0×10^3 cfu mL^{-1} were added. After 60 min contact, 100 μL of bacterial solution was plated on to an agar plate. Three parallel groups were set for each sample. The agar plate was incubated at 37 °C for 24 h. The bacterial-killing rate was calculated based on the number of colonies as per the following equation:

$$\text{Bactericidal efficiency} = (a_0 - a)/a_0$$

where a_0 is the bacterial quantity of the bare groups, and a means the bacterial quantity of the samples, such as PU, PU-PDA, and PU-PDA/Zn-0.08 films.

The morphology of *Escherichia coli* (*E. coli*) and *Staphylococcus aureus* (*S. aureus*) after touching the PU, PU-PDA and PU-PDA/Zn films was characterized by a slide-climbing method. Here, 500 μL of bacteria (*E. coli* or *S. aureus*) diluted to 1.0×10^4 cfu mL^{-1} was incubated overnight with a glass slide in each well of a 48-well plate at 37 °C. Subsequently, the PU, PU-PDA, and PU-PDA/Zn films with a diameter of 1.75 cm were added to the 48-well plates for 12 h at 37 °C. After that, the planktonic bacteria were removed and washed three times with sterile PBS buffer solution. The bacteria-covered glass slides were fixed with 2.5% glutaraldehyde overnight, and dehydrated through the use of 25, 50, 75, and 100 wt% ethanol–water solutions (10 min each time). After drying, the obtained samples were subjected to SEM observation.

Moreover, live/dead staining was performed to explore the survival ability of the bacteria in contact with the surfaces of the PU, PU-PDA, and PU-PDA/Zn films. The aforementioned bacteria-climbed glass slides were gently flushed by sterile water (made by the laboratory, with high-temperature

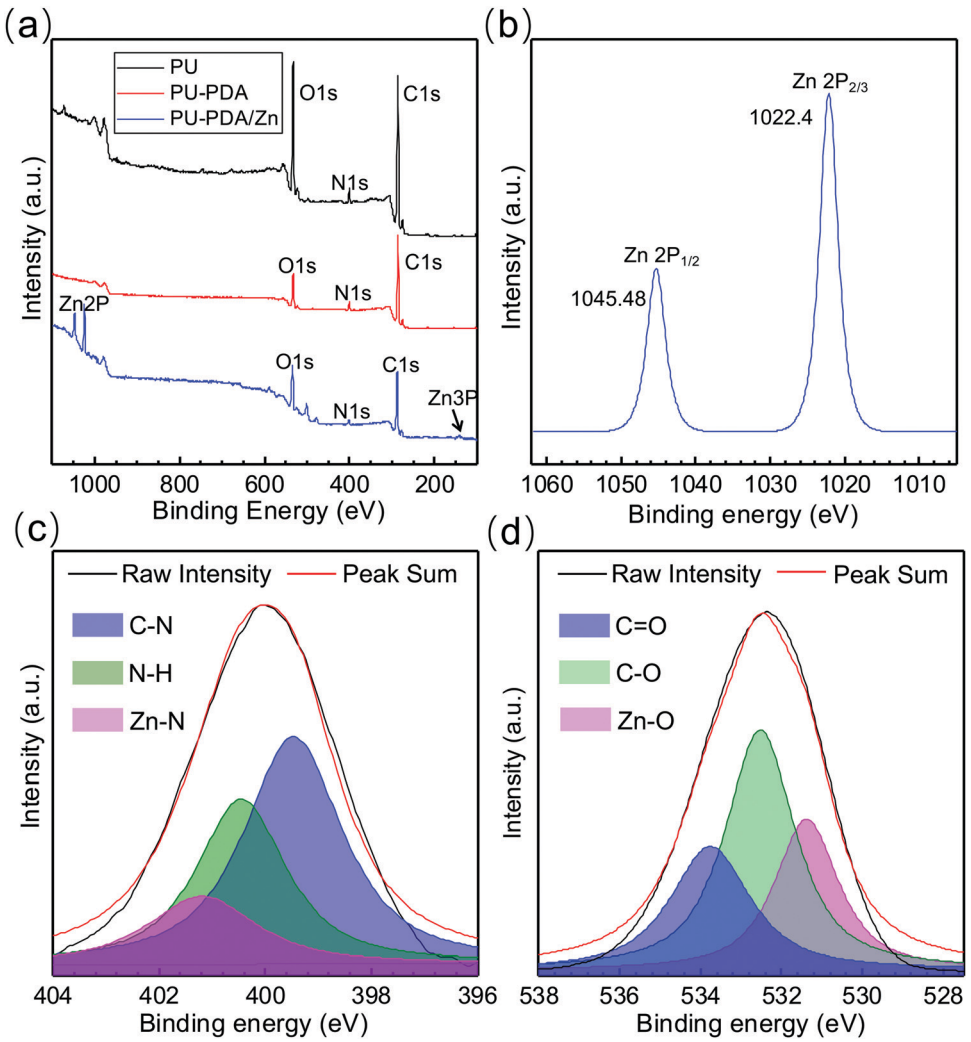

Fig. 3 (a) Full XPS spectra of PU, PU-PDA, PU-PDA/Zn-0.08 films. (b)–(d) High-resolution XPS spectra of Zn 2p (b), N 1s (c), and O 1s (d) in PU-PDA/Zn-0.08 films.

sterilization performed with deionized water), and dyed by 150 μL live/dead staining (Invitrogen by Thermo Fisher Scientific) for 20 min (for the preparation method, see the manufacturer's instructions for use). The dyed glass slides were observed under a fluorescence microscope.

Results and discussion

Characterization and forming mechanism

To ensure the effect of the zinc content with the PDA on the morphologies and hydrophilicity, we increased the zinc ammonium concentration in the reaction mixture to obtain different PU-PDA/Zn samples. Fig. 2(a1)–(a4) show the SEM images of the surface of the PU-PDA/Zn films prepared using the 0.2, 0.15, 0.08, and 0.05 mol L^{-1} concentrations, respectively. When the concentration of zinc ammonium was 0.2 mol L^{-1}, the surface appeared to have a pyknotic coating (Fig. 2(a1)). A honeycombed structure was formed as the concentration of the zinc ammonium decreases to 0.08 and 0.05 mol L^{-1}, which was considered to be a result of the appropriate proportion of zinc in the PDA polymer. After coating with PDA/Zn, the water contact angle of the modified PU surface was significantly lower compared to that of the original PU film, which was 83.5° (Fig. S1, ESI†). Interestingly, when the water contact angle of the PU-PDA/Zn film decreased to below 10°, the honeycombed structure appeared (Fig. 2(b3)). When further lowering the concentration of zinc ammonium to 0.05 mol L^{-1} in the reaction mixture, although the honeycombed structure of the PDA/Zn coating could still be formed, the contact angle of the PU-PDA/Zn-0.05 surface increased to 18.9°, which may be due to the increased relative proportion of PDA polymer. The PDA surface on the PU was confirmed to be without superhydrophilicity (Fig. S1, ESI†).

Further, we reveal the time-dependent growing process of the PDA/Zn-0.08 coating as its contact angle was the lowest among the PU-PDA/Zn samples prepared by different zinc ammonium concentrations. The SEM images of the surface of the PU-PDA/Zn-0.08 undergoing 1, 2, 6, and 24 h reactions are shown in Fig. 2(c). During the first 2 h, sparse nanowires appeared on the surface of the PU films (Fig. 2(c1) and (c2)). As the reaction time went on, the nanowires continually grew and became intertwined to form a honeycombed structure (Fig. 2(c3) and (c4)). The nanostructure of the PDA/Zn-0.08 enhanced the water wettability, as confirmed by the water contact angle (Fig. 2(d)). After 24 h coating, the water contact angle of the PU-PDA/Zn-0.08 was lowered to 7.4°. Such superhydrophilicity is helpful for antifouling,[20] as the hydrophobic protein and bacteria cannot adhere on a superhydrophilic surface.[43–45]

The XPS spectra were obtained to further evaluate the coordination interaction of the Zn^{2+} in the polydopamine. As shown in Fig. 3(a), Zn 2p and Zn 3p peaks were found in the spectrum of the PU-PDA/Zn film, which were absent in the XPS spectra of the PU and PU-PDA films. Combined with the SEM image of the PU-PDA/Zn film (Fig. 1(d)) that was completely different to the surface morphologies of PU and PU-PDA films (Fig. S2, ESI†), the XPS result indicated that the zinc was trapped in the coating materials. Moreover, we examined the Zn 2p region in the PU-PDA/Zn film, which exhibited two peaks at 1022.4 and 1045.48 eV corresponding to the doublet from Zn $2p_{3/2}$ and Zn $2p_{1/2}$, respectively (Fig. 3(b)). The binding energies in the Zn 2p regions of the PU-PDA/Zn film were close to the characteristic peaks of Zn in ZIF-8, which possessed a zeolitic imidazole framework consisting of Zn^{2+} cations bridged by imidazolate linkers,[46] while they were significantly higher than those of the previously reported values of ZnO.[47] The Zn may coordinate with PDA *via* Zn–N bonds like the Zn in ZIF-8, which was verified by the nitrogen 1s XPS spectra.[46] The binding energy of 399.5 eV was attributed to the C–N bonds, one with 400.45 eV was assigned to N–H bonds; the two peaks were also exhibited in the N 1s XPS spectra of the PU and PU-PDA films (Fig. S3, ESI†). Interestingly, Fig. 3(c) displayed a new peak in the nitrogen 1s XPS spectra of the PU-PDA/Zn film that was spotted at 401.02 eV. This binding energy was assigned to the formation of new bonds between Zn atoms and N atoms from

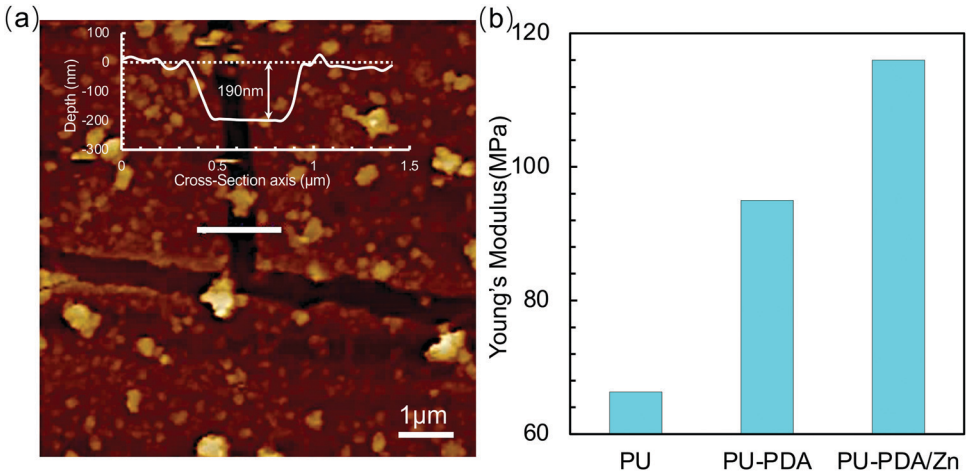

Fig. 4 (a) AFM images of PU-PDA/Zn-0.08 film (insert: the depth profiles across the PDA/Zn-0.08 surface). (b) Young's modulus of the surface of the PU, PU-PDA, and PU-PDA/Zn-0.08 films tested by AFM.

PDA.[48] Besides, the formation of zinc–oxygen (Zn–O) bonds was also observed in the O 1s XPS spectra of the PU-PDA/Zn film (Fig. 3(d)). The binding energies at 532.54 and 533.77 eV corresponded to C–O and C═O bonds, while the binding energy of 531.39 eV was suggested to be due to Zn–O bonds as the O atoms also existed in the polydopamine.[49] The XPS results confirmed the formation of Zn–N and Zn–O bonds in the coordination interaction of the Zn^{2+} with the polydopamine.

The FT-IR results verified the XPS analysis (Fig. S4, ESI†). The characteristic peak of the PU-PDA film at 1438 cm^{-1} was attributed to the bending vibration of N–H bonds, while the peak at 1350 cm^{-1} corresponded to the bending vibration of O–H bonds, and the peak at 1275 cm^{-1} corresponded to the stretching vibration of C–N bonds. Those are characteristic peaks of polydopamine. With the Zn coordinating with polydopamine, a blue-shift of the N–H and C–N characteristic peaks occurred. The FT-IR peak related to O–H bonds decreased due to the formation of Zn–O bonds. Based on the results of XPS and FT-IR, it is suggested that the Zn^{2+} built Zn–N and Zn–O bonds with polydopamine to form several possible structures (Fig. S5, ESI†).

The PDA/Zn coating was stable when immersed in water, but quite unstable in the acid solution with pH 1 (Fig. S6, ESI†). When rinsing under flowing water at 100 mL min^{-1}, the PDA/Zn coating was slightly washed out, but still with its nanostructure maintained. When increasing the flowing water to 500 mL min^{-1}, the structure of the PDA/Zn coating was obviously eroded (Fig. S6, ESI†).

In order to determine the thickness and surface features of the PDA/Zn coating, the surface of the PDA/Zn film was tested by atomic force microscopy in the fault zone.[50] The result showed that the PDA/Zn coating was *ca.* 190 nm thick (Fig. 4(a)). The elasticity properties of the PU, PU-PDA, and PU-PDA/Zn-0.08 surfaces were tested by atomic force microscopy (AFM), a method whereby a material's surface is indented using a soft cantilever under a contact mode. The Young's modulus (E) of the PU-PDA/Zn-0.08 film was 116 MPa, which was obviously greater than that of PU and PU-PDA (Fig. 4(b)). The values of E for the soft hydrated materials are usually reported with great distinction when measured using different methods.[50,51] Using atomic force microscopy, the value of the PU film was measured as 66.3 MPa, and the value for PU-PDA was 72.8 MPa. These results showed that the PU-PDA/Zn-0.08 film was stiffer. The stiffness of the surface influences numerous behaviours of the live cell, such as cell proliferation, migration, and differentiation.[52–54] The stiff surface of the PU-PDA/Zn-0.08 film may go against the live cell adhesion and proliferation, which is completely positive for antibiofouling.

Antibiofouling property and biotoxicity test

The platelet adhesion and protein adsorption testing results confirmed the foregoing verdict. For the PU film, the platelets obtained from the whole blood of New Zealand white rabbit were inclined to adhere on to the surface (Fig. 5(a)). The pseudopodia of the platelets were noteworthily extended on the surface of the PU film, indicating the platelets were in an

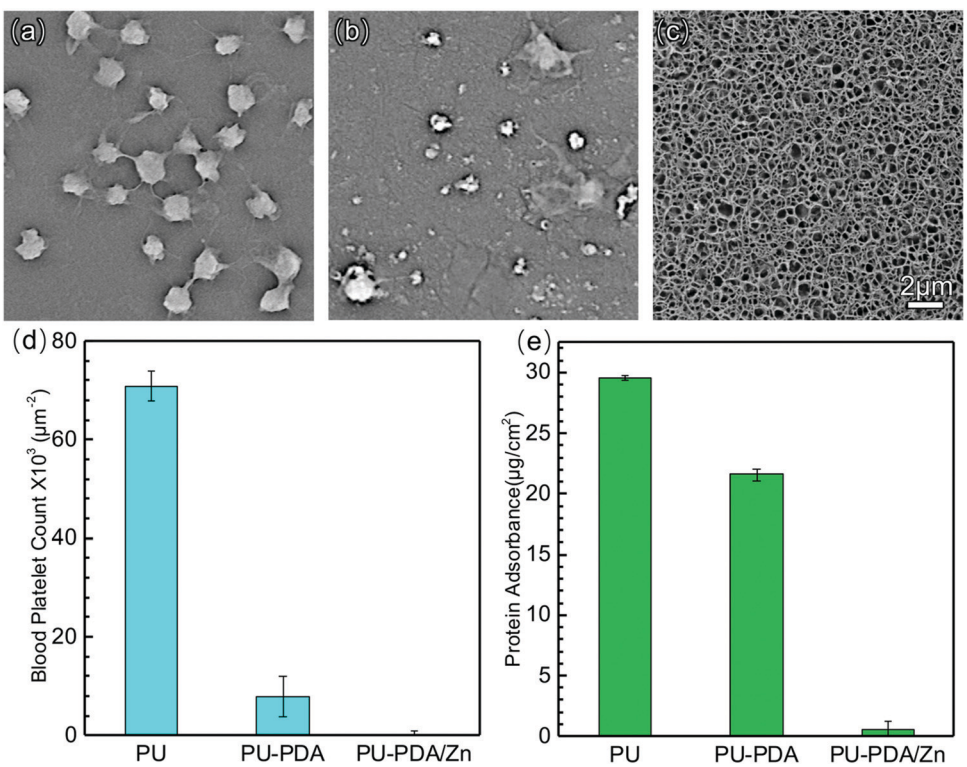

Fig. 5 SEM images of the platelets adhered on PU (a), PU-PDA (b), PU-PDA/Zn-0.08 (c). Blood platelets count from the SEM images (d). Adsorption of BSA on PU, PU-PDA, and PU-PDA/Zn-0.08 (e).

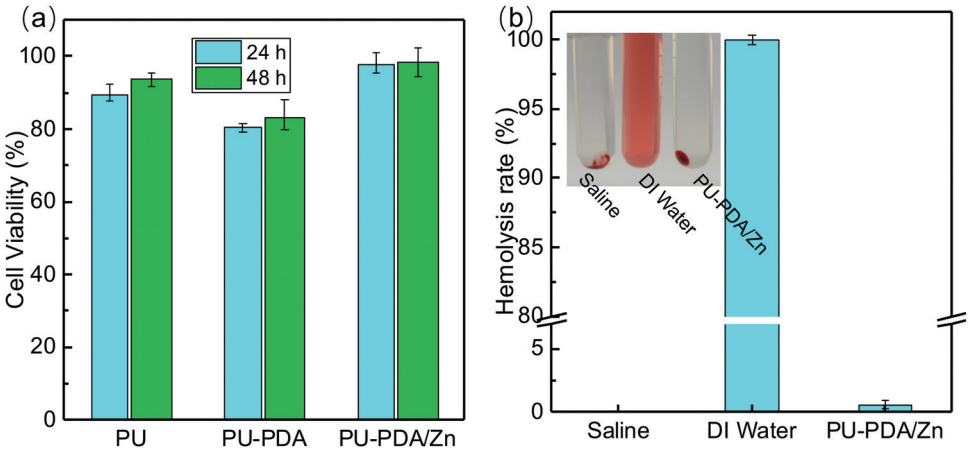

Fig. 6 Cell viability of L929 cells incubated with PU, PU-PDA, and PU-PDA/Zn-0.08 for 24 h and 48 h (a). Haemolysis rate of PU-PDA/Zn-0.08 interacted with whole blood using DI water as the positive control and saline as the negative control (b). The inset in (b) is a digital photo of the groups.

activated state. By contrast, scattered platelets were found on the surface of the PU-PDA films, but still with extending pseudopodia (Fig. 5(b)). However, there were fewer platelets on the surface of the PU-PDA/Zn-0.08 films (Fig. 5(c) and Fig. S7, ESI†). The density of the platelets adhered to the surface was counted from the SEM images (Fig. 5(d)). The results

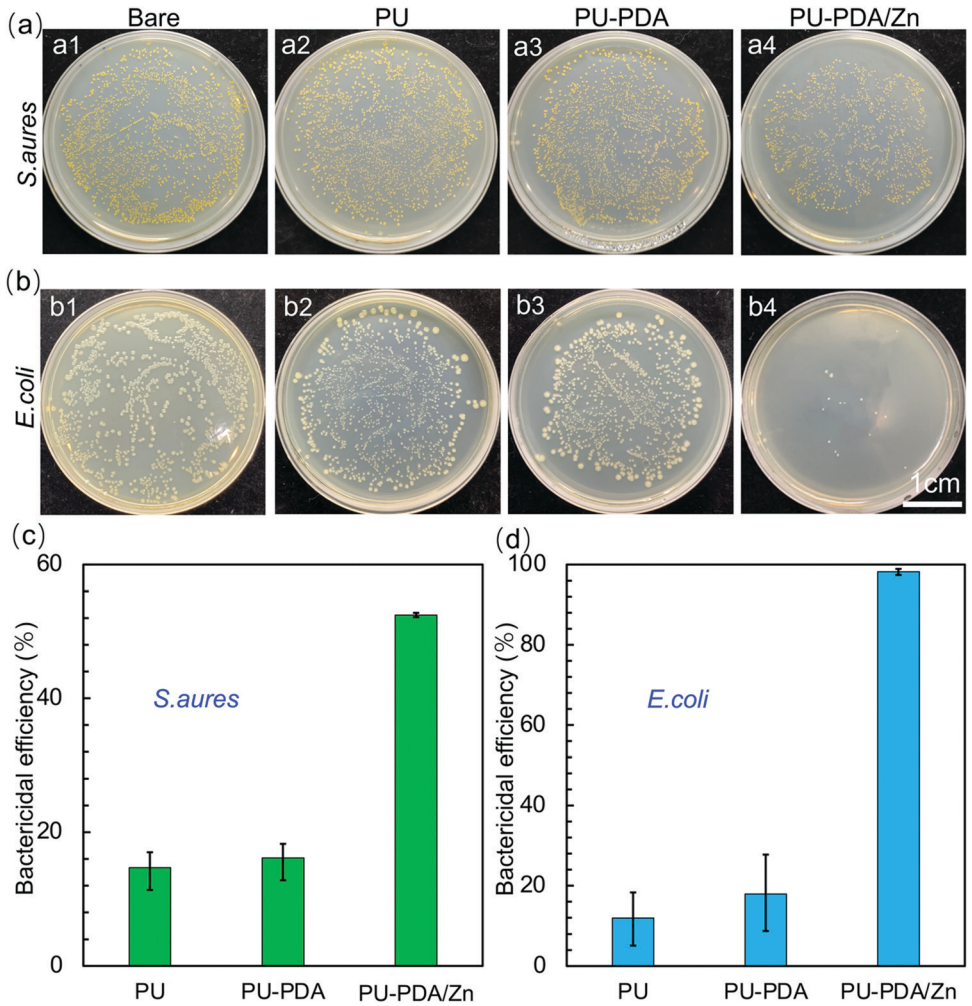

Fig. 7 Bacterial growth photographs of *S. aureus* (a) and *E. coli* (b) without treatment (a1, b1) or treated with PU (a2, b2), PU-PDA (a3, b3), PU-PDA/Zn-0.08 films (a4, b4). Antibacterial efficiency of PU, PU-PDA, and PU-PDA/Zn-0.08 films against *S. aureus* (c) and *E. coli* (d).

suggested the platelets were unwilling to adhere on the surface of the PU-PDA/Zn-0.08 film. There are two factors to consider here: one factor is the superhydrophilicity of the surface of the PU-PDA/Zn-0.08 films, whereby live cells generally adhere to hydrophobic surfaces but not on highly hydrated hydrophilic surfaces;[55–57] and the other factor is the stiffness of the surface of PU-PDA/Zn films, which was higher than those of the PU film and PU-PDA film. The normal cells were attached to essentially rigid materials, such as tissue culture plastic or glass coverslips, often *via* adsorbed matrix protein,[58] which was reluctant to adhere on to PU-PDA/Zn-0.08. To evidence this, we used BSA (67 kDa) to simulate the protein absorption assay.[59,60] The BSA protein adsorption capacities of the PU, PU-PDA, and PU-PDA/Zn-0.08 films are shown in Fig. 5(d). The values of the protein absorbance of PU and PU-PDA were 29.6 and 21.7 μg cm^{-2}, which were apparently higher than that of the PU-PDA/Zn-0.08 film (only 1.21 μg cm^{-2}). Considering the nanostructure of the PDA/Zn-0.08 coating, the protein absorbance to the specific surface area was lower than 1.21 μg cm^{-2}. From the results of both the platelet adhesion and protein adsorption, the PU-PDA/Zn film with antibiofouling property had low biological contamination, which is an essential element for the potential application of anti-coagulation and anti-thrombogenesis in artificial blood catheters.

To reveal the suitability of the PU-PDA/Zn film for further biological applications, the biotoxicity was further analyzed *via* cytotoxicity experiments and haemolysis tests. For the cytotoxicity investigation, the L929 mouse fibroblasts were incubated with the PU, PU-PDA, and PU-PDA/Zn-0.08 film for 24 h and 48 h, respectively. The cell viabilities were tested using the Cell Counting Kit-8 (CCK-8) array (Fig. 6(a)), which was approximately 100% for the PU-PDA/Zn-0.08 film. The results indicated that the materials in our strategy have a satisfactory biocompatibility. Fig. 6(b) shows the haemolysis rate of the PU-PDA/Zn-0.08 film, which was lower than 5% using saline as the negative group and DI water as the positive group. When the whole blood from New Zealand white rabbit contacted with the PU-PDA/Zn-0.08 film, no hemoglobin rupture occurred (inset of Fig. 6(b)), which showed that the PU-PDA/Zn-0.08 film was biosafe to the blood. The results confirmed the effective antibiofouling property and the ignorable biotoxicity of the PU-PDA/Zn-0.08 film.

Antibacterial performances

To assess the antibacterial performance of the PU-PDA/Zn films, *S. aureus* and *E. coli*, the most prevalent species of Gram-positive and Gram-negative bacteria, respectively, were employed *via* the spread plate method. Fig. 7(a) and (b) are

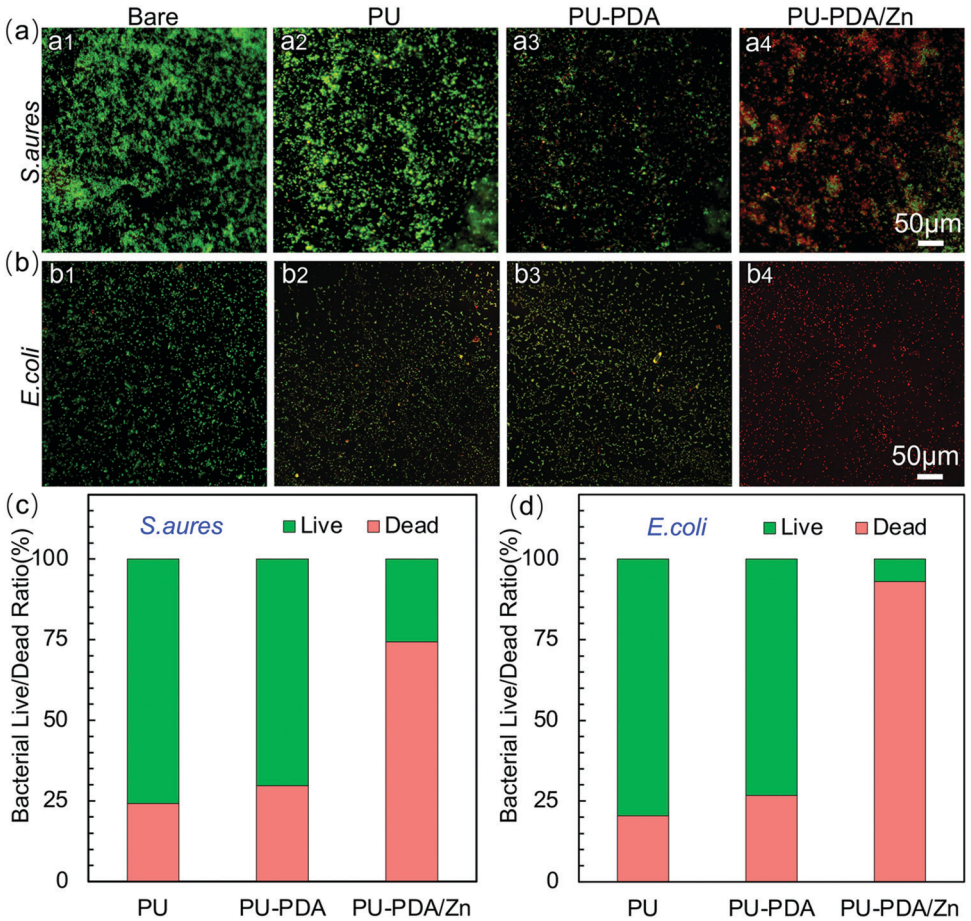

Fig. 8 Fluorescence images of *S. aureus* (a) and *E. coli* (b) after contact sterilization of PU, PU-PDA, and PU-PDA/Zn-0.08 films. Bacterial live/dead ratio of *S. aureus* (c) and *E. coli* (d) from the fluorescence images counted by ImageJ software.

photographs of *S. aureus* and *E. coli* reproducing on the agar plates for 24 h after 60 min contacting with the PU, PU-PDA, and PU-PDA/Zn-0.08 films, separately. The PU and PU-PDA films demonstrated no antibacterial efficacy, because the bacteria continually multiplied after 60 min contacting with the PU and PU-PDA. Nevertheless, a considerable number of *S. aureus* colonies were detected in Fig. 7(a4), while there was a prominent reduction of *E. coli* colonies for the PU-PDA/Z-0.08 samples (Fig. 7(b4)). The bactericidal efficiency was calculated from the number of the colonies. The bactericidal efficiency of the Gram-positive *S. aureus* of the PU, PU-PDA, and PU-PDA/Zn-0.08 films were 14.6%, 16.1%, and 52.5%, respectively, showing a degree of antibacterial performance of PU-PDA/Zn-0.08 films against *S. aureus*. As expected, the bactericidal efficiencies of the PU and PDA film against *E. coli* were low at 11.9% and 17.9%, respectively, which shows the bactericidal effect to *E. coli* of the two samples was is feeble. Differently, the bactericidal efficiency of the PU-PDA/Zn-0.08 film against *E. coli* was high at 98.2% (Fig. 7(c)), which showed that the Zn^{2+} did have a notably positive antimicrobial performance to Gram-negative bacteria.

Moreover, the survival rates of *E. coli* and *S. aureus* after treatment with the PU, PU-PDA, and PU-PDA/Zn films were observed by live–dead staining, in which the viable bacteria were green and the dead bacteria were red (Fig. 8(a) and (b)). In comparison to the strong green fluorescence of *S. aureus* and *E. coli* in the control group, green fluorescence of the two bacteria was still observed, indicating that a large number of viable bacteria existed on the PU and PU-PDA surfaces. However, for the bacteria contacting with PDA/Zn coated on the PU, the green fluorescence was significantly decreased, while the red fluorescence was greatly increased, which indicated that the PU-PDA/Zn film had excellent antibacterial properties. The bacterial live/dead ratio of PU, PU-PDA, and PU-PDA/Zn against *S. aureus* as well as *E. coli* were calculated by the ImageJ software from the fluorescence images to show the semiquantitative antibacterial efficiency (Fig. 8(c) and (d)). The antibacterial efficiencies of Gram-positive *S. aureus* of the PU, PU-PDA, and PU-PDA/Zn-0.08 films were 24.4%, 29.7%. and 74.2%, while the antibacterial efficiencies of Gram-negative *E. coli* of the PU, PU-PDA, and PU-PDA/Zn-0.08 films were 20.4%, 26.7%, and 93.0%, respectively. These results were consistent with that from the colonies numbers (Fig. 7).

Because of the antibacterial attachment performance of the PDA/Zn coating, few bacteria were attached on the surface (Fig. 9(a), (b) and Fig. S8, ESI†). To show the morphologies of *E. coli* and *S. aureus* after touching the PU, PU-PDA, and PU-PDA/Zn samples, the bacteria were fixed on glass slides and observed by SEM. As shown in Fig. 9(c) and (d), both *S. aureus* and *E. coli* in the control group displayed smooth surfaces and no visible damage of the bacterial membrane (Fig. 9(c1) and (d1)), while the morphologies of *S. aureus* after PU and PU-PDA

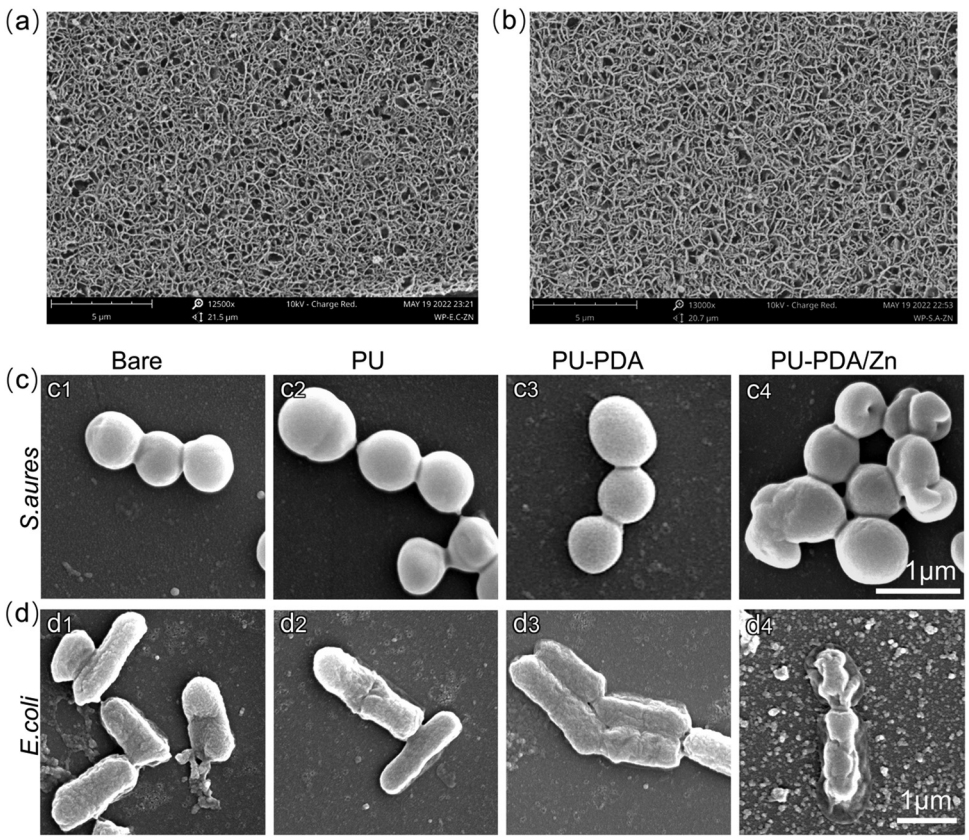

Fig. 9 SEM images to show *S. aureus* (a) and *E. coli* (b) attachment on the PU-PDA/Zn-0.08 films. SEM images of *S. aureus* (c) and *E. coli* (d) fixed on the glass slides after contact sterilization of PU, PU-PDA, and PU-PDA/Zn-0.08 films.

treatment were hardly changed and showed a globose shape with a smooth surface (Fig. 9(c2) and (c3)), and *S. aureus* after contact with the PU-PDA/Zn film possessed collapsed morphologies. Combining the above results with Fig. 7(c), 8(c) and 9(c), it signified that the PDA/Zn coating partly inhibited the *S. aureus* growth through contact killing (Fig. 9(c4)). Even the clubbed *E. coli* contacted with PU and PU-PDA films still maintained the original morphology without remarkable deformation (Fig. 9(d2) and (d3)). Specifically, the *E. coli* suffered from a bacterial membrane collapse, resulting in a distorted morphology after PU-PDA/Zn film treatment (Fig. 9(d4)). The Zn^{2+} broke the bacterial membrane by irreversible Zn(II)–protein binding, leading to severe cytoplasm leakage,[41,61] which indicated the prominent antibacterial effect of the PDA/Zn coating on the PU substrate.

Conclusions

In summary, we demonstrated a biofouling-resistant and antibacterial surface that constituted zinc-coordinated polydopamine (PDA/Zn). The zinc ions bonded with the –N and –O sites of polydopamine to form nanowires at first. As the nanowires continued growing and intertwining, they finally formed a honeycombed structure that was affected by the proportion of the zinc ions to the polydopamine. The PDA/Zn coating was verified to have a nanostructure and superhydrophilicity, which could oppose the adhesion of the platelets and protein. Combined with the ignorable biotoxicity and haemolysis effect, it is proposed that the PDA/Zn could be coated on an artificial blood catheter and dialysis membrane for anti-coagulation and anti-thrombogenesis effects. Moreover, the PDA/Zn coating here enabled sterilizing against *E. coli* and *S. aureus* bacteria because of the ability of zinc ions, which could break the bacterial membrane due to the irreversible binding of Zn(II)–protein in the cell membrane, which leads to severe cytoplasm leakage. Considering these results together, the PDA/Zn coating with a honeycombed structure is highly favourable for biological applications, such as the functionalization of artificial catheters and membranes.

Author contributions

L. Z. and P. W. conceived and designed the study. P. W. performed the experiments. All the authors discussed the results and contributed to the data interpretation. L. Z. and P. W. wrote the manuscript and all the authors commented on the manuscript.

Conflicts of interest

There are no conflicts to declare.

Acknowledgements

The authors gratefully acknowledge the support from the National Natural Science Foundation of China (22022810), the Scientific and Technological Department of Sichuan Province, China (No. 2020YFG0105) and Sichuan University (2020SCUNG112).

References

1 Y. H. Joung, *Int. Neurourol. J.*, 2013, **17**, 98–106.
2 C. R. Arciola, D. Campoccia and L. Montanaro, *Nat. Rev. Microbiol.*, 2018, **16**, 397–409.
3 V. Narasimhan, R. H. Siddique, J. O. Lee, S. Kumar, B. Ndjamen, J. Du, N. Hong, D. Sretavan and H. Choo, *Nat. Nanotechnol.*, 2018, **13**, 512–519.
4 R. O. Darouiche, *Clin. Infect. Dis.*, 2001, **33**, 1567–1572.
5 I. Francolini, C. Vuotto, A. Piozzi and G. Donelli, *APMIS*, 2017, **125**, 392–417.
6 M. T. Kalathottukaren and J. N. Kizhakkedathu, in *Hemocompatibility of Biomaterials for Clinical Applications*, ed. C. A. Siedlecki, Woodhead Publishing, 2018, pp. 29–49.
7 L. C. Xu, J. W. Bauer and C. A. Siedlecki, *Colloids Surf., B*, 2014, **124**, 49–68.
8 I. H. Jaffer, J. C. Fredenburgh, J. Hirsh and J. I. Weitz, *J. Thromb. Haemostasis*, 2015, **13**, S72–S81.
9 Y. Z. Qiu, A. C. Brown, D. R. Myers, Y. Sakurai, R. G. Mannino, R. Tran, B. Ahn, E. T. Hardy, M. F. Kee, S. Kumar, G. Bao, T. H. Barker and W. A. Lam, *Proc. Natl. Acad. Sci. U. S. A.*, 2014, **111**, 14430–14435.
10 N. Rabin, Y. Zheng, C. Opoku-Temeng, Y. X. Du, E. Bonsu and H. O. Sintim, *Future Med. Chem.*, 2015, **7**, 493–512.
11 I. Guzman-Soto, C. McTiernan, M. Gonzalez-Gomez, A. Ross, K. Gupta, E. J. Suuronen, T. F. Mah, M. Griffith and E. I. Alarcon, *iScience*, 2021, **24**, 102443.
12 S. Ahmed and R. O. Darouiche, *Adv. Exp. Med. Biol.*, 2015, **831**, 137–146.
13 J. D. Bryers, *Biotechnol. Bioeng.*, 2008, **100**, 1–18.
14 S. Singh, S. K. Singh, I. Chowdhury and R. Singh, *Open Microbiol. J.*, 2017, **11**, 53–62.
15 M. D. Macia, E. Rojo-Molinero and A. Oliver, *Clin. Microbiol. Infect.*, 2014, **20**, 981–990.
16 I. Banerjee, R. C. Pangule and R. S. Kane, *Adv. Mater.*, 2011, **23**, 690–718.
17 A. M. C. Maan, A. H. Hofman, W. M. de Vos and M. Kamperman, *Adv. Funct. Mater.*, 2020, **30**, 2000936.
18 A. L. Hook, C. Y. Chang, J. Yang, J. Luckett, A. Cockayne, S. Atkinson, Y. Mei, R. Bayston, D. J. Irvine, R. Langer, D. G. Anderson, P. Williams, M. C. Davies and M. R. Alexander, *Nat. Biotechnol.*, 2014, **32**, 592.
19 M. Cloutier, D. Mantovani and F. Rosei, *Trends Biotechnol.*, 2015, **33**, 637–652.
20 J. Drelich, E. Chibowski, D. D. Meng and K. Terpilowski, *Soft Matter*, 2011, **7**, 9804–9828.
21 Z. X. Huang and H. Ghasemi, *Adv. Colloid Interface Sci.*, 2020, **284**, 102264.
22 H. Qiu, K. Feng, A. Gapeeva, K. Meurisch, S. Kaps, X. Li, L. Yu, Y. K. Mishra, R. Adelung and M. Baum, *Prog. Polym. Sci.*, 2022, **127**, 101516.
23 S. F. Chen, L. Y. Li, C. Zhao and J. Zheng, *Polymer*, 2010, **51**, 5283–5293.
24 J. J. Liu, S. X. Qu, Z. G. Suo and W. Yang, *Natl. Sci. Rev.*, 2021, **8**, nwaa254.
25 L. Y. Xie, F. Hong, C. X. He, C. F. Ma, J. H. Liu, G. Z. Zhang and C. Wu, *Polymer*, 2011, **52**, 3738–3744.

26 J. Baggerman, M. M. J. Smulders and H. Zuilhof, *Langmuir*, 2019, **35**, 1072–1084.
27 Y. X. Zhang, Y. L. Liu, B. P. Ren, D. Zhang, S. W. Xie, Y. Chang, J. T. Yang, J. Wu, L. J. Xu and J. Zheng, *J. Phys. D: Appl. Phys.*, 2019, **52**, 403001.
28 L. Zheng, H. S. Sundaram, Z. Wei, C. Li and Z. Yuan, *React. Funct. Polym.*, 2017, **118**, 51–61.
29 M. Kobayashi, Y. Terayama, H. Yamaguchi, M. Terada, D. Murakami, K. Ishihara and A. Takahara, *Langmuir*, 2012, **28**, 7212–7222.
30 F. J. Xu, K. G. Neoh and E. T. Kang, *Prog. Polym. Sci.*, 2009, **34**, 719–761.
31 Y. Higaki, M. Kobayashi, D. Murakami and A. Takahara, *Polym. J.*, 2016, **48**, 325–331.
32 W. Ahmed, Z. Zhai and C. Gao, *Mater. Today Bio*, 2019, **2**, 100017.
33 S. Y. Wu, J. M. Xu, L. Y. Zou, S. L. Luo, R. Yao, B. N. Zheng, G. B. Liang, D. C. Wu and Y. Li, *Nat. Commun.*, 2021, **12**, 3303.
34 M. C. Jennings, K. P. C. Minbiole and W. M. Wuest, *ACS Infect. Dis.*, 2015, **1**, 288–303.
35 D. Druvari, N. D. Koromilas, G. C. Lainioti, G. Bokias, G. Vasilopoulos, A. Vantarakis, H. Baras, N. Dourala and J. K. Kallitsis, *ACS Appl. Mater. Interfaces*, 2016, **8**, 35593–35605.
36 P. Makvandi, R. Jamaledin, M. Jabbari, N. Nikfarjam and A. Borzacchiello, *Dent. Mater.*, 2018, **34**, 851–867.
37 R. Dastjerdi and M. Montazer, *Colloids Surf., B*, 2010, **79**, 5–18.
38 A. Singh and A. K. Dubey, *ACS Appl. Bio Mater.*, 2018, **1**, 3–20.
39 M. Korani, E. Ghazizadeh, S. Korani, Z. Hami and A. Mohammadi-Bardbori, *Eur. J. Nanomed.*, 2015, **7**, 51–62.
40 M. Salomaki, L. Marttila, H. Kivela, T. Ouvinen and J. Lukkari, *J. Phys. Chem. B*, 2018, **122**, 6314–6327.
41 R. David, *Nat. Rev. Microbiol.*, 2012, **10**, 4.
42 C. A. McDevitt, A. D. Ogunniyi, E. Valkov, M. C. Lawrence, B. Kobe, A. G. McEwan and J. C. Paton, *PLoS Pathog.*, 2011, **7**, e1002357.
43 L. H. Li, L. Yang, Y. B. Liao, H. C. Yu, Z. Liang, B. Zhang, X. R. Lan, R. F. Luo and Y. B. Wang, *Chem. Eng. J.*, 2020, **402**, 126196.
44 S. M. Oliveira, N. M. Alves and J. F. Mano, *J. Adhes. Sci. Technol.*, 2014, **28**, 843–863.
45 T. Ishizaki, N. Saito and O. Takai, *Langmuir*, 2010, **26**, 8147–8154.
46 M. Hayashi, D. N. T. Lee, M. D. de Mello, J. A. Boscoboinik and M. Tsapatsis, *Angew. Chem., Int. Ed.*, 2021, **60**, 9316–9320.
47 J. Gao and A. V. Teplyakov, *Catal. Today*, 2014, **238**, 111–117.
48 M. Tu, B. Z. Xia, D. E. Kravchenko, M. L. Tietze, A. J. Cruz, I. Stassen, T. Hauffman, J. Teyssandier, S. De Feyter, Z. Wang, R. A. Fischer, B. Marmiroli, H. Amenitsch, A. Torvisco, M. D. Velasquez-Hernandez, P. Falcaro and R. Ameloot, *Nat. Mater.*, 2021, **20**, 93–99.
49 Y. Xiang, C. Mao, X. Liu, Z. Cui, D. Jing, X. Yang, Y. Liang, Z. Li, S. Zhu, Y. Zheng, K. W. K. Yeung, D. Zheng, X. Wang and S. Wu, *Small*, 2019, **15**, 1900322.
50 M. D. A. Norman, S. A. Ferreira, G. M. Jowett, L. Bozec and E. Gentleman, *Nat. Protoc.*, 2021, **16**, 2418–2449.
51 C. T. McKee, J. A. Last, P. Russell and C. J. Murphy, *Tissue Eng., Part B*, 2011, **17**, 155–164.
52 N. D. Evans, C. Minelli, E. Gentleman, V. LaPointe, S. N. Patankar, M. Kallivretaki, X. Y. Chen, C. J. Roberts and M. M. Stevens, *Eur. Cells Mater.*, 2009, **18**, 1–14.
53 A. J. Engler, S. Sen, H. L. Sweeney and D. E. Discher, *Cell*, 2006, **126**, 677–689.
54 R. Krishnan, D. D. Klumpers, C. Y. Park, K. Rajendran, X. Trepat, J. van Bezu, V. W. M. van Hinsbergh, C. V. Carman, J. D. Brain, J. J. Fredberg, J. P. Butler and G. P. V. Amerongen, *Am. J. Physiol.: Cell Physiol.*, 2011, **300**, C146–C154.
55 B. D. Ratner, T. Horbett, A. S. Hoffman and S. D. Hauschka, *J. Biomed. Mater. Res.*, 1975, **9**, 407–422.
56 B. R. McAuslan and G. Johnson, *J. Biomed. Mater. Res.*, 1987, **21**, 921–935.
57 T. Okano, N. Yamada, M. Okuhara, H. Sakai and Y. Sakurai, *Biomaterials*, 1995, **16**, 297–303.
58 D. E. Discher, P. Janmey and Y. L. Wang, *Science*, 2005, **310**, 1139–1143.
59 K. Ishihara, K. Fukumoto, Y. Iwasaki and N. Nakabayashi, *Biomaterials*, 1999, **20**, 1545–1551.
60 K. Ishihara, K. Fukumoto, Y. Iwasaki and N. Nakabayashi, *Biomaterials*, 1999, **20**, 1553–1559.
61 J. Ye, B. Li, M. Li, Y. Zheng, S. Wu and Y. Han, *Acta Biomater.*, 2020, **107**, 313–324.